Journal of Solid State Chemistry **153,** 321–329 (2000)
doi:10.1006/jssc.2000.8777, available online at http://www.idealibrary.com on IDEAL®

Structure and Thermoelectric Properties of Ba_6Ge_{25-x}, $Ba_6Ge_{23}Sn_2$, and $Ba_6Ge_{22}In_3$: Zintl Phases with a Chiral Clathrate Structure

Sung-Jin Kim,*,[1] Siqing Hu,† Ctirad Uher,† Tim Hogan,‡ Baoquan Huang,§ John D. Corbett,§ and Mercouri G. Kanatzidis*,[2]

*Department of Chemistry, Michigan State University, East Lansing, Michigan 48824; †Department of Physics, University of Michigan, Ann Arbor, Michigan 48109; ‡Department of Electrical & Computer Engineering, Michigan State University, East Lansing, Michigan 48824; and §Ames Laboratory and Department of Chemistry, Iowa State University, Ames, Iowa 50011

Received December 27, 1999; revised May 12, 2000; accepted May 18, 2000; published online July 26, 2000

A single phase of Ba_6Ge_{25-x} ($x \sim 1$) was obtained from a direct element combination reaction in a sealed graphite tube at 830°C. Its structure was determined by single-crystal X-ray diffraction methods. Ba_6Ge_{25-x} adopts the chiral cubic space group $P4_132$ (No. 213) with dimensions of $a = 14.5483(2)$ Å and $Z = 4$. The structure consists of helical chains of Ba atom-centered pentagonal dodecahedra, $Ba@Ge_{20}$, and zeolite-like cages formed by those chains. There are vacancies distributed over the Ge sites giving a composition of Ba_6Ge_{24}, in which charge balance according to the Zintl formalism is retained. The compound therefore satisfies the classical Zintl concept. Polycrystalline ingots of Ba_6Ge_{25-x} showed an electrical conductivity of 2000 S/cm and a Seebeck coefficient of -18 μV/K at room temperature. An anomalous broad transition in the electrical conductivity and Seebeck coefficient was observed at ~ 100 K. $Ba_6Ge_{23.32}Sn_{1.68}$ and $Ba_6Ge_{21.93}In_{3.07}$ as ternary derivatives of Ba_6Ge_{25-x} were also synthesized and their structural and physical properties compared with those of Ba_6Ge_{25-x}.

***Key Words*: chiral clathrate; thermoelectric; zintl phase; phonon gas; electron crystal.**

INTRODUCTION

A stimulating idea in the field of thermoelectric materials is the concept of PGEC ("phonon-glass, electron-crystal") proposed by Slack (1). PGEC materials should possess the low thermal conductivity of a glass, but maintain the high electronic mobilities of crystalline semiconductors. It has been suggested that PGEC behavior could be seen in systems with heavy cations "rattling" inside oversized lattice cavities, which could create ideal conditions for extensive thermal phonon scattering that leads to very low thermal conductivity (2,3). As potential PGEC materials, are considered the clathrate-type class of Zintl compounds, in which their oversize cages are filled with heavy electropositive cation rattlers. In these compounds the anionic frameworks are covalently bonded providing a medium for high carrier mobility. Indeed interest in this class of compounds has escalated recently (2d,e).

There are two well-known clathrate-type structures, A_8X_{46} clathrate(I)- and A_8X_{136} clathrate(II)-type structures, where A is an alkali or alkaline earth metal and X is an element or elements from groups 12–14 (4). The X elements build open tetrahedral networks having pentagonal dodecahedra and tetrakaidecahedra for A_8X_{46}, and pentagonal dodecahedra and hexakaidecahedra for A_8X_{136}. In both clathrates, two different cages are condensed in three dimensions by face sharing. The alkali or alkaline earth metal atoms are found in the center of the polyhedra. However, the chiral cubic compounds, $Ba_6In_4Ge_{21}$ and K_xSn_{25} ($x \sim 6$–8), can also be considered as clathrate-type compounds (5). In these systems distorted pentagonal dodecahedra are the only building blocks. These dodecahedra are helically condensed by sharing three pentagonal faces and are interconnected through external bonds. As this clathrate-like structure forms, one sees not only pentagonal dodecahedra in helical chains, but also, open channels around the chains filled with electropositive metals.

In the past, research on Zintl-type compounds mainly concentrated on exploring the extent of the validity of the Zintl concept itself and focused primarily on the systems with relatively light atoms in the framework (6,7). The great majority of Zintl compounds are reported to be air and moisture sensitive and their physical properties are not well studied. Given the apparent relationship of the clathrate phases to the large class of Zintl compounds, the latter seem an attractive group in which to search for new thermoelectric materials. These must be air and moisture stable and

[1] Permanent address: Department of Chemistry, Ewha Woman's University, Seoul, Korea 120–750.
[2] To whom corresondence should be addressed. E-mail: Kanatzidis@cem.msu.edu.

0022-4596/00 $35.00

this maybe achieved in Zintl compounds with heavier elements and divalent electropositive cations. Recently, we synthesized the environmentally stable Zintl phase $Ba_4In_8Sb_{16}$ which has a complex structure and encouraging thermoelectric properties (8). Our attempts to synthesize new air-stable Zintl phases resulted in the discovery of Ba_6Ge_{25-x} ($x = 1$), which is isostructural with K_6Sn_{25} and $Ba_6In_4Ge_{21}$ (5). Here we describe the synthesis, crystal structure, and properties of Ba_6Ge_{25-x} ($x = 1$) along with some ternary derivatives. A preliminary assessment of their thermoelectric properties including electrical conductivity, thermopower, and thermal conductivity is reported.

EXPERIMENTAL SECTION

Synthesis. Ba_6Ge_{25-x} was first identified in reactions intended to synthesize a new clathrate type analogue with Ba_8Ge_{46} composition. The single crystal of Ba_6Ge_{25-x} used in the structure determination resulted from the reaction of a mixture of the two elements (Ba, Aldrich, 99%; Ge, Cerac, chips, 99.999%) in a molar ratio of 8:46. The reaction mixtures were placed in closed graphite tubes and sealed into evacuated silica tubes. The sealed mixtures were heated slowly to 830°C, kept at that temperature for 1 day, and subsequently cooled to room temperature over 1 day. These reactions led to the formation of a few chunky black crystals along with silvery featureless pieces. Semiquantitative microprobe analysis (EDS) on single crystals gave $Ba_{24.0(2)}Ge_{96.0(2)}$. Once the stoichiometry was determined from the X-ray single-crystal structure analysis, Ba_6Ge_{25-x} was prepared rationally as a single phase, starting from the exact stoichiometric ratio of Ba/Ge = 1/4 by inductive heating at 1200°C for 10 min. The X-ray powder patterns of the bulk sample agreed well with the powder pattern calculated from its single-crystal data.

The single crystals of $Ba_6In_xGe_{25-x}$ ($x \sim 3$) and $Ba_6Sn_xGe_{25-x}$ ($x \sim 2$) used in the structure determination were obtained from reactions of a mixture of three elements (Ba, Aldrich, chunk under oil, 99%, Sn, Cerac, shots, 99.999%; Ge, Cerac, chips, 99.999%; In, Cerac, chunk, 99.999%) in molar ratios of Ba:In:Ge = 6:4:21 and Ba:Sn:Ge = 6:2:23, respectively. The reaction mixtures were placed in graphite tubes and sealed in evacuated silica tubes. The sealed mixtures were heated slowly to 900°C, kept at that temperature for 1 day, and subsequently cooled to room temperature over 1 day. The reactions led to the formation of a few silvery chunky crystals along with brittle featureless pieces. Semiquantitative microprobe analysis on single crystals of $Ba_6In_xGe_{25-x}$ and $Ba_6Sn_xGe_{25-x}$ gave $Ba_6In_{3.07}Ge_{22.1}$ and $Ba_6Sn_{1.68}Ge_{23.1}$, respectively.

Electron microscopy. Semiquantitative microprobe analysis of the compounds was performed with a JEOL JSM-35C scanning electron microscope (SEM) equipped with a Tracor Northern energy dispersive spectroscopy (EDS) detector. Data were acquired using an accelerating voltage of 20 kV.

Differential thermal analysis. Differential thermal analysis (DTA) was performed with a Shimadzu DTA-50 thermal analyzer. The ground sample (~20.0 mg total mass) was sealed in a carbon-coated silica ampoule under vacuum. A silica ampoule containing alumina powder of equal mass was sealed and placed on the reference side of the detector. The sample was heated to 950°C at 10°C/min and kept there for 10 min, followed by cooling at −10°C/min to 50°C. The stability and reproducibility of the sample were monitored by running multiple heating and cooling cycles. The residue of the DTA experiment was examined with X-ray powder diffraction.

Charge-transport and thermal conductivity measurements. The electrical conductivities of polycrystalline ingots of Ba_6Ge_{25-x}, $Ba_6In_xGe_{25-x}$, and $Ba_6Sn_xGe_{25-x}$ were measured using a four-probe method (9). The polycrystalline ingots were obtained from a reaction using graphite as a container and they were ground to cylindrical shape with ~2 mm radius and ~5 mm length for measurements. Thermal conductivity and thermopower were determined using a longitudinal steady-state method over the temperature range 4–300 K. In this case samples were attached (using either a low-melting-point solder or silver-loaded epoxy) to the cold tip of the cryostat, while the other end of the samples was provided with a small strain gauge resistor (thin film) which serves as a heater. The temperature differences across the samples were measured using a differential chromel–constantan thermocouple.

Crystallographic studies. A black chunky crystal of Ba_6Ge_{25-x} with dimensions of $0.05 \times 0.05 \times 0.05\ mm^3$ was mounted on the end of a glass fiber. A Siemens SMART Platform CCD diffractometer was used to collect intensity data using graphite-monochromatized Mo$K\alpha$ radiation. The data were collected over a full sphere of reciprocal space up to 57° in 2θ. The individual frames were measured with an ω rotation of 0.3° and an acquisition time of 60 seconds. To check for crystal stability, at the end of data collection procedure, the initial 50 frames of data were measured again and compared. No crystal decay was detected. The SMART software (10) was used for data acquisition and SAINT (11) for data extraction and reduction. The absorption correction was performed empirically using SADABS (12). The unit cell parameters were obtained from least-squares refinement using randomly chosen 600 reflections from a full sphere of reciprocal space up to 57° in 2θ. The cubic cell parameters and calculated volume were $a = 14.5483(2)$ Å and 3079.19 Å^3 for Ba_6Ge_{25-x}. The observed Laue symmetry and systematic extinctions were indicative of the two enantiomorphic space groups: $P4_332$ (No. 212) or $P4_132$

(No. 213). The initial positions of all atoms were obtained from direct methods. Both space groups were tried for refinements and the statistically better solutions were chosen on the basis of R values and number of variables. The structure was refined by full-matrix least-squares techniques with the SHELXTL (13) crystallographic program. Once all atoms were located, the occupancies of successive atoms were allowed to vary, and refinements led to significant changes in the occupation factors of Ge sites. Only one Ge site remained in full occupancy. The final cycle of refinement performed on F_o^2 with 55 variables and 1291 averaged reflections converged to residuals $wR2$ ($F_o^2 > 0$) of 0.0788. On the other hand, the conventional R index based on reflections having $F_o > 2\sigma(F_o)$ was 0.0338. A difference Fourier synthesis calculated with phases based on the final parameters showed a maximum peak of 4.484 e/Å^3 at 0.85 Å from the Ge(6) atom and a maximum hole of -1.733 e/Å^3 at 0.21 Å from the Ge(6) atom. The structures of both $Ba_6In_xGe_{25-x}$ and $Ba_6Sn_xGe_{25-x}$ were similarly refined. At first only Ge atoms were assigned. Then the occupancy factors of all Ge atoms were allowed to vary. The occupancy factors of certain Ge sites increased above 1.0 and these sites were assigned to In and Sn, respectively. We observed no signs of ordering in Ge/Sn or Ge/In sites; instead the Sn or In atoms appear randomly distributed on Ge sites in both compounds. When the occupancy factors of the disordered sites were allowed to vary no significant changes were noted. Therefore, the possibility of partial occupation on these sites was discounted. Complete data collection parameters and details of structure solutions and refinement results of three compounds are given in Table 1. Final atomic positions, atomic displacement parameters (ADPs), and anisotropic displacement parameters are given in Tables 2–7.

TABLE 1
Selected Data from the Single-Crystal Refinements

Empirical formula	Ba_6Ge_{24}	$Ba_6Ge_{23.32}Sn_{1.68}$	$Ba_6Ge_{21.93}In_{3.07}$
Formula weight	10,264.80	10,515.84	11,073.32
Temperatue (K)	293(2)	293(2)	293(2)
Wavelength ($\lambda = K\alpha$, Å)	0.71073	0.71073	0.71073
Space group	$P4_132$	$P4_332$	$P4_332$
Lattice constant a, (Å)	14.5483(2)	14.7073(8)	14.7409(6)
Volume (Å^3)	3079.19(7)	3181.3(3)	3203.1(2)
Z	4	4	4
Density, ρ_{calc} (g/cm^3)	5.536	5.489	5.741
Absorption coefficent (mm^{-1})	30.530	23.276	29.600
Reflections collected	22,140	22,335	26,146
Data/restraints/ parameters	1291/0/55	1350/0/56	1351/0/59
R_{int}	0.058	0.081	0.064
Final R indices $[F_o^2 > 2\sigma(F_o^2)]^a$	$R1 = 0.0338$, $wR2 = 0.0782$	$R1 = 0.0462$, $wR2 = 0.1156$	$R1 = 0.0181$, $wR2 = 0.0396$
R indices ($F_o^2 > 0$)	$R1 = 0.0357$, $wR2 = 0.0788$	$R1 = 0.0570$, $wR2 = 0.1201$	$R1 = 0.0212$, $wR2 = 0.0400$
Largest diff. peak/hole (e/Å^3)	4.484 and -1.733	5.101 and -1.850	0.643 and -0.612

[a] $R1 = [\Sigma||F_o| - |F_c||]/\Sigma|F_o|$. $wR2 = \{[\Sigma w(|F_o| - |F_c|)^2/[\Sigma w(F_o^2)^2]]\}^{1/2}$. $w = \sigma_F^{-2}$.

RESULTS AND DISCUSSION

Structure

The binary A_8X_{46} members (A = alkali metal; X = Si, Ge, Sn) have been reported as semiconductors, e.g., K_8Ge_{46} 4(b). Structural analysis suggests that they are best described as $A_8X_{46}\square_2$, where $\square$ is a vacancy. Various ternary compounds with the formula $A_8M_nX_{46-n}$ ($n = 8, 16$; A = alkali metal; M = group 12 or 13; X = group 14), such as $Ba_8In_{16}Ge_{30}$ and $Ba_8Zn_8Ge_{38}$, are also known. These are typically Zintl phases and, therefore, semiconductors (6). Also, some derivatives of $A_8M_nX_{46-n}$ ($n = 16$) with vacancies in the anionic framework, such as $Ba_8(In_4Ge_9\square_3)Ge_{30}$ ($\square$ = vacancy on Ge site) have been reported, where nine M sites are substituted with X elements and three sites remain vacant. In clathrate(I)-type structures, the dodecahedra and tetrakaidecahedra share all 12 and 14 faces with other polyhedra. However, in Ba_6Ge_{25-x} only 3 out of 12 pentagonal faces of each dodecahedron are shared with other like polyhedra. As a result the structure of Ba_6Ge_{25-x} is more open than the A_6X_{46}-type structure and thus provides the potential of extensive Ba atom rattling.

Figure 1 shows how the pentagonal dodecahedra form helical chains by sharing two pentagonal faces. In the full structure of Ba_6Ge_{25-x}, three helical chains running along three axis directions are connected both by sharing three

TABLE 2
Atomic Coordinates (×10^4) and Equivalent Isotropic Displacement Parameters (Å^2×10^3) for Ba_6Ge_{24}

Atom	Site	x	y	z	U(eq)[a]	Occ. (%)
Ba (1)	8c	601 (1)	601 (1)	601 (1)	10 (1)	1
Ba (2)	4a	6250	8750	1250	18 (1)	1
Ba (3)	12d	1883 (1)	4383 (1)	1250	48 (1)	1
Ge (1)	24e	9996 (1)	2966 (1)	428 (1)	5 (1)	0.938 (7)
Ge (2)	12d	8307 (1)	807 (1)	1250	5 (1)	0.944 (9)
Ge (3)	24e	8634 (1)	9154 (1)	845 (1)	7 (1)	0.980 (6)
Ge (4)	8c	9246 (1)	9246 (1)	9246 (1)	6 (1)	1
Ge (5)	24e	1257 (1)	2597 (1)	9348 (1)	6 (1)	0.972 (7)
Ge (6)	8c	9690 (1)	4690 (1)	310 (1)	22 (1)	0.911 (12)

[a] $U_{(eq)}$ is defined as one-third of the trace of the orthogonalized U_{ij} tensor.

TABLE 3
Atomic Coordinates (×10⁴) and Equivalent Isotropic Displacement Parameters (Å²×10³) for $Ba_6Ge_{23.32}Sn_{1.68}$

Atom	*x*	*y*	*z*	*U* (eq)[a]	Occ. (%)
Ba (1)	5622 (1)	9378 (1)	622 (1)	18 (1)	1
Ba (2)	1250	1250	1250	35 (1)	1
Ba (3)	1925 (3)	9434 (3)	− 1030 (2)	47 (1)	0.50
Ge (1)	7960 (1)	9568 (1)	28 (1)	16 (1)	1
Ge (2)	9758 (1)	9758 (1)	9758 (1)	36 (1)	0.52 (3)
Sn (2)	9758 (1)	9758 (1)	9758 (1)	36 (1)	0.48 (3)
Ge (3)	3342 (1)	9158 (1)	1250	18 (1)	1
Ge (4)	7586 (1)	0623 (1)	1290 (1)	17 (1)	1
Ge (5)	4262 (1)	738 (1)	− 738 (1)	19 (1)	0.64 (2)
Sn (5)	4262 (1)	738 (1)	− 738 (1)	19 (1)	0.36 (2)
Ge (6)	3532 (1)	822 (1)	892 (1)	19 (1)	1

[a] $U_{(eq)}$ is defined as one-third of the trace of the orthogonalized U_{ij} tensor.

faces and by joining through external Ge(4)–Ge(4) bonds. Figure 2 shows a pentagonal dodecahedron centered with a Ba^{2+} ion (endohedral). The three shared faces are indicated and the Ge sites are labeled. There are two kinds of Ge atom environments: 8 Ge atoms have trigonal pyramidal coordination and the remaining 17 Ge atoms have tetrahedral coordination. There are no large differences in the spread of the Ge–Ge bond lengths between the three-bonded and four-bonded Ge atoms (Table 8). The Ge–Ge bond lengths vary between 2.475(2)–2.581(2) Å, and are similar to the Ge–Ge lengths at 2.454–2.543 Å in $Ba_8Ga_{16}Ge_{30}$, and slightly larger than the 2.445 Å bond length of Ge–Ge in elemental germanium 4(e).

TABLE 4
Atomic Coordinates (×10⁴), Equivalent Isotropic Displacement Parameters (Å²×10³), and Occupancies for $Ba_6Ge_{21.93}In_{3.07}$

Atom	*x*	*y*	*z*	*U* (eq)[a]	Occ. (%)
Ba (1)	5580 (1)	9420 (1)	580 (1)	13 (1)	1
Ba (2)	1250	1250	1250	25 (1)	1
Ba (3)	1872 (2)	9363 (2)	8911 (2)	36 (1)	0.50
In (1)	7959 (1)	9583 (1)	9973 (1)	12 (1)	0.277 (6)
Ge (1)	7959 (1)	9583 (1)	9973 (1)	12 (1)	0.723 (6)
In (2)	9680 (1)	9680 (1)	9680 (1)	27 (1)	0.063 (10)
Ge (2)	9680 (1)	9680 (1)	9680 (1)	27 (1)	0.937 (10)
In (3)	3268 (1)	9232 (1)	1250	16 (1)	0.264 (7)
Ge (3)	3268 (1)	9232 (1)	1250	16 (1)	0.736 (7)
In (4)	7602 (1)	0683 (1)	1241 (1)	13 (1)	0.016 (6)
Ge (4)	7602 (1)	0683 (1)	1241 (1)	13 (1)	0.984 (6)
In (5)	4246 (1)	0754 (1)	9246 (1)	14 (1)	0.191 (9)
Ge (5)	4246 (1)	0754 (1)	9246 (1)	14 (1)	0.809 (9)
Ge (6)	3541 (1)	0874 (1)	849 (1)	20 (1)	1

[a] $U_{(eq)}$ is defined as one-third of the trace of the orthogonalized U_{ij} tensor.

TABLE 5
Anisotropic Displacement Parameters (Å²×10³) for Ba_6Ge_{24}

	*U*11	*U*22	*U*33	*U*23	*U*13	*U*12
Ba (1)	10 (1)	10 (1)	10 (1)	0 (1)	0 (1)	0 (1)
Ba (2)	18 (1)	18 (1)	18 (1)	− 6 (1)	6 (1)	− 6 (1)
Ba (3)	18 (1)	18 (1)	107 (1)	− 2 (1)	2 (1)	6 (1)
Ge (1)	5 (1)	4 (1)	6 (1)	− 1 (1)	1 (1)	1 (1)
Ge (2)	6 (1)	6 (1)	5 (1)	− 1 (1)	1 (1)	2 (1)
Ge (3)	7 (1)	6 (1)	9 (1)	1 (1)	1 (1)	− 1 (1)
Ge (4)	6 (1)	6 (1)	6 (1)	− 2 (1)	− 2 (1)	− 2 (1)
Ge (5)	6 (1)	6 (1)	7 (1)	0 (1)	2 (1)	0 (1)
Ge (6)	22 (1)	22 (1)	22 (1)	1 (1)	1 (1)	− 1 (1)

Note. The anisotropic displacement factor exponent takes the form $-2\pi^2[h^2a^{*2}U11 + \ldots + 2hka^*b^*U12]$.

The distances from the endohedral Ba(1) atoms to the Ge atoms of the Ge_{20} cage are in a range of 3.3938–4.004(11) Å, which indicates that there are large distortions from the ideal pentagonal dodecahedral geometry. The deformation of the dodecahedra is due to the displacement of the trigonal pyramidal atoms Ge(3) and Ge(6) from the ideal dodecahedral structure. Atom Ge(3) is displaced from the ideal dodecahedral net toward Ba(2) and Ba(3) at 3.4259(11) and 3.3357(11) Å, respectively. Also, the dodecahedron is slightly stretched so that the Ge(6) vertex approaches Ba(3) at 3.500(1) Å. These relatively short bond lengths are due to strong Coulombic interactions between the Ba atoms and the lone pair of electrons of the pyramidal Ge(3) and Ge(6) atoms. The Ba–Ge distances in the dodecahedral cage in $Ba_8Ga_{16}Ge_{30}$ range between 3.445 (×8)–3.554 (×12) Å with an average of 3.51 Å, which suggests little distortion from the ideal dodecahedron 4(e).

TABLE 6
Anisotropic Displacement Parameters (Å²×10³) for $Ba_6Ge_{23.32}Sn_{1.68}$

	*U*11	*U*22	*U*33	*U*23	*U*13	*U*12
Ba (1)	18 (1)	18 (1)	18 (1)	0 (1)	0 (1)	0 (1)
Ba (2)	35 (1)	35 (1)	35 (1)	− 2 (1)	− 2 (1)	− 2 (1)
Ba (3)	43 (2)	30 (1)	68 (3)	3 (2)	10 (2)	8 (1)
Ge (1)	16 (1)	15 (1)	17 (1)	− 1 (1)	1 (1)	2 (1)
Ge (2)	36 (1)	36 (1)	36 (1)	1 (1)	1 (1)	1 (1)
Sn (2)	36 (1)	36 (1)	36 (1)	1 (1)	1 (1)	1 (1)
Ge (3)	18 (1)	18 (1)	19 (1)	2 (1)	2 (1)	− 5 (1)
Ge (4)	17 (1)	18 (1)	16 (1)	− 3 (1)	0 (1)	0 (1)
Ge (5)	19 (1)	19 (1)	19 (1)	2 (1)	− 2 (1)	2 (1)
Sn (5)	19 (1)	19 (1)	19 (1)	2 (1)	− 2 (1)	2 (1)
Ge (6)	16 (1)	15 (1)	26 (1)	− 1 (1)	1 (1)	2 (1)

Note. The anisotropic displacement factor exponent takes the form $-2\pi^2[h^2a^{*2}U11 + \ldots + 2hka^*b^*U12]$.

TABLE 7
Anisotropic Displacement Parameters ($Å^2 \times 10^3$) for $Ba_6Ge_{21.93}In_{3.07}$

	*U*11	*U*22	*U*33	*U*23	*U*13	*U*12
Ba (1)	13 (1)	13 (1)	13 (1)	− 1 (1)	1 (1)	− 1 (1)
Ba (2)	25 (1)	25 (1)	25 (1)	9 (1)	9 (1)	9 (1)
Ba (3)	25 (1)	23 (1)	61 (2)	6 (1)	4 (1)	6 (1)
In (1)	13 (1)	12 (1)	12 (1)	− 1 (1)	2 (1)	0 (1)
Ge (1)	13 (1)	12 (1)	12 (1)	− 1 (1)	2 (1)	0 (1)
In (2)	27 (1)	27 (1)	27 (1)	2 (1)	2 (1)	2 (1)
Ge (2)	27 (1)	27 (1)	27 (1)	2 (1)	2 (1)	2 (1)
In (3)	17 (1)	17 (1)	13 (1)	1 (1)	1 (1)	− 8 (1)
Ge (3)	17 (1)	17 (1)	13 (1)	1 (1)	1 (1)	− 8 (1)
In (4)	13 (1)	15 (1)	12 (1)	− 3 (1)	− 1 (1)	0 (1)
Ge (4)	13 (1)	15 (1)	12 (1)	− 3 (1)	− 1 (1)	0 (1)
In (5)	14 (1)	14 (1)	14 (1)	1 (1)	− 1 (1)	1 (1)
Ge (5)	14 (1)	14 (1)	14 (1)	1 (1)	− 1 (1)	1 (1)
Ge (6)	13 (1)	23 (1)	24 (1)	− 5 (1)	− 1 (1)	2 (1)

Note. The anisotropic displacement factor exponent takes the form $-2\pi^2[h^2a^{*2}U11 + \ldots + 2hka^*b^*U12]$.

The ADPs of Ba(1) ion in Table 2 are comparable to those of Ge atoms. The larger atomic displacements of Ba(2), compared to those of Ba(1), seem to be due to the low coordination number of the six Ge atoms at 3.4259(11) Å.

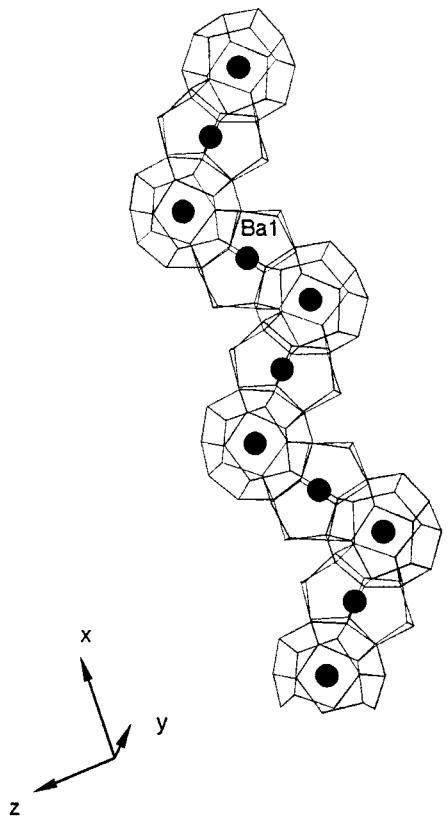

FIG. 1. Helical chain of Ge dodecahedra projected along the [100] direction.

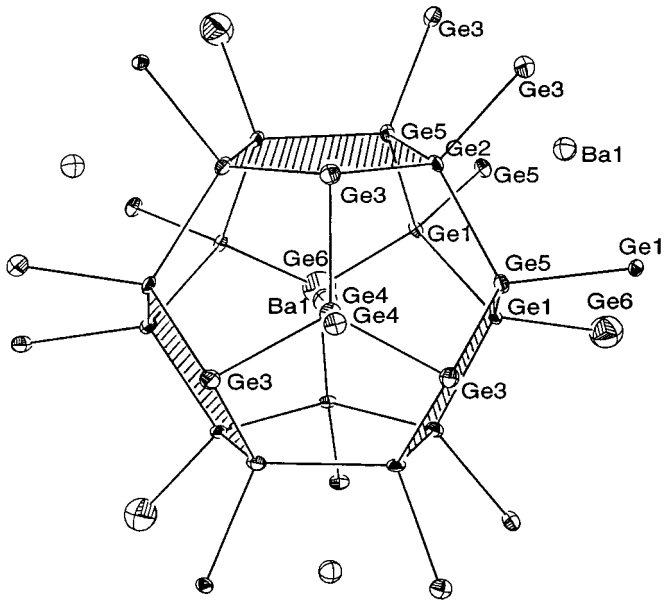

FIG. 2. ORTEP representation and atomic labeling of a dodecahedral building block (80% probability ellipsoids) of Ba_6Ge_{24}. This block extends by sharing its three faces to make helical chains along the three directions and by interconnecting with other dodecahedral building blocks.

The Ba(2) atoms have a distorted octahedral geometry, see Fig. 3b. The distances between Ba(3) and the closest 20 germanium atoms are in the range of 3.335(1)–4.426(2) Å. Except for two short Ba(3)–Ge(3) bonds at 3.3353(14) Å, the channels are substantially oversized for the Ba(3) atoms, as suggested by the rather large ADPs. Figure 3 shows a zeolytic-like framework with channels following the direction of helices. Atoms Ba(2) and Ba(3) lie along the channels and the shortest Ba(2)–Ba(3) distance is 4.6317(4) Å. The large ADPs associated with the trigonal pyramidal Ge(6) atoms seem to be correlated with the correspondingly large ADPs of its nearest Ba(3) neighbor. The angle of Ge(1)–Ge(6)–Ge(1), 96.73(8)°, is smaller than other germanium-centered angles and it is due to the repulsion from the lone pair of electrons.

If all Ba and Ge sites were fully occupied, the composition would be Ba_6Ge_{25}. The partial occupancies observed in five germanium sites. However, result in the composition Ba_6Ge_{24}. Only the Ge(4) sites, located on *C*3 symmetry, are fully occupied and these Ge atoms connect to two neighboring dodecahedra by external Ge–Ge bonds. The composition $Ba_{24.0(2)}Ge_{96.0(2)}$, as converged in the structural refinement, is in excellent agreement with the analytical data from EDS. An important common feature of all three compounds described here is that the ADPs of the Ba atoms in the channels are much larger than those located inside the pentagonal dodecahedral Ge_{20} cage. Therefore any "rattling" of Ba atoms, if present, would be happening not inside the cages but rather in the more open spaces outside.

TABLE 8
Selected Bond Distances (Å) and Angles (deg) in Ba_6Ge_{24}

Ba(1)–Ge(1) (×3)	3.4947 (14)	Ge(1)–Ge(1)	2.581 (2)
Ge(2) (×3)	3.4813 (10)	Ge(5)	2.475 (2)
Ge(4) (×1)	3.415 (2)	Ge(5)	2.545 (2)
Ge(5) (×3)	3.3938 (11)	Ge(6)	2.552 (2)
Ge(5) (×3)	3.5588 (11)	Ge(2)–Ge(3) (×2)	2.4976 (14)
Ge(1) (×3)	3.565 (2)	Ge(5) (×2)	2.5614 (14)
Ge(3) (×3)	3.668 (2)	Ge(3)–Ge(2)	2.4976 (14)
Ge(6)	4.004 (11)	Ge(4)	2.5494 (12)
Ba(2)–Ge(3) (×6)	3.4259 (11)	Ge(5)	2.536 (2)
Ge(6) (×2)	3.931 (2)	Ge(4)–Ge(3) (×3)	2.5494 (12)
Ge(2) (×2)	4.232 (2)	Ge(4)	2.500 (4)
Ba(3)–Ge(1) (×2)	3.636 (2)	Ge(5)–Ge(1) (×2)	2.545 (2)
Ge(1) (×2)	3.6602 (13)	Ge(2)	2.5615 (14)
Ge(3) (×2)	3.3357 (14)	Ge(3)	2.536 (2)
Ge(5) (×2)	3.6681 (11)	Ge(6)–Ge(1) (×3)	2.552 (2)
Ge(6) (×2)	3.5002 (10)		
Ge(5) (×2)	3.904 (2)		
Ge(4) (×2)	4.039 (2)		
Ge(2) (×2)	4.195 (2)		
Ge(3) (×2)	4.283 (2)		
Ge(3) (×2)	4.426 (2)		

Ge(5)–Ge(1)–Ge(5)	101.30 (4)	Ge(3)–Ge(4)–Ge(3)	113.40 (4)
Ge(5)–Ge(1)–Ge(6)	107.46 (7)	Ge(1)–Ge(5)–Ge(3)	111.34 (5)
Ge(5)–Ge(1)–Ge(1)	109.51 (6)	Ge(1)–Ge(5)–Ge(1)	100.62 (4)
Ge(6)–Ge(1)–Ge(1)	111.65 (6)	Ge(3)–Ge(5)–Ge(1)	116.25 (5)
Ge(3)–Ge(2)–Ge(3)	108.07 (8)	Ge(1)–Ge(5)–Ge(2)	110.58 (5)
Ge(3)–Ge(2)–Ge(5)	110.40 (3)	Ge(3)–Ge(5)–Ge(2)	108.60 (5)
Ge(2)–Ge(3)–Ge(5)	100.80 (5)	Ge(1)–Ge(6)–Ge(1)	96.73 (8)
Ge(2)–Ge(3)–Ge(4)	102.63 (5)	Ge(3)–Ge(3)–Ge(3)	101.88 (5)
Ge(4)–Ge(4)–Ge(3)	105.19 (5)		

A key question to be addressed is whether Ba_6Ge_{24} has any composition range. We prepared several samples in which the 6:24 ratio was allowed to vary $\pm 10\%$. The lattice parameters did not show any significant changes. The best product was obtained when the Ba_6Ge_{24} composition was used. Compositions such as Ba_6Ge_{25} showed Ba_6Ge_{24} plus elemental Ge. It would appear that despite the vacancies found in Ba_6Ge_{24}, the compound is almost a line phase with $x = 1$. The site occupancy factors of the Ba atoms were constant and at the theoretically expected full occupancy level.

Based on the Zintl concept, the formal charges of $Ba_6In_4Ge_{21}$ are described as $[Ba^{2+}]_6[(3b)Ge^-]_8[(4b)In^-]_4[(4b)Ge]_{13}$. This is a valence-precise compound and therefore it is a semiconductor. However, K_6Sn_{25} has been described as $[K^+]_6[(3b)Sn^-]_8[(4b)Sn]_{17}$ and it appears to be an electron-deficient compound. Depending on the reaction conditions, K_6Sn_{25} was found to be nonstoichiometric in the composition range of K_6Sn_{25}–K_8Sn_{25}. If stoichiometric Ba_6Ge_{25} phase existed, the formal charge of three and four-bonded germanium atoms can be assigned as Ge^- and Ge^0, respectively, and it can be presented as $[Ba^{2+}]_6[(Ge^-)_8(Ge^0)_{17}]$. Therefore, it would have four extra electrons per formula giving rise to metallic properties. However, the observed composition Ba_6Ge_{24} suggests that one Ge vacant site per formula $Ba_6Ge_{24}\square_1$ compensates four extra electrons giving a valence-precise compound and potential semiconducting properties.

Thermal Analysis and Spectroscopic Characterization

The compound Ba_6Ge_{24} is stable in room temperature and air, and melts congruently at 818°C. Pure single phase could be obtained by directly melting the two elements in an induction heater. The band gap of the compound however could not be observed spectroscopically in the mid-IR region (4000–400 cm^{-1}) probably due to interference from defect energy levels. Those defect sites seem also to affect the transport properties.

Charge and Thermal Transport Measurements

The electrical conductivity and thermoelectric power of polycrystalline ingots of Ba_6Ge_{25-x} were measured as a function of temperature. A rather high electrical conductivity of $\sim$2000 S/cm was observed at room temperature comparable to the values of well-known semimetals such as Bi_2Te_3 (2.2×10^3 S/cm) (14). The data shown in Fig. 4 show a strong temperature variation in the conductivity in between 300–150 K. At $\sim$150 K there is an anomalous minimum in the data and below that temperature the conductivity rises to $\sim$1200 S/cm at 5 K. Also, an anomalous transition in the Seebeck coefficient was observed at similar temperature. The anomalous transition seems to be related with the defects on Ge sites.

The thermopower (Seebeck coefficient) for Ba_6Ge_{24} is -18 μV/K at room temperature and shows little dependence down to $\sim$130 K. Below this temperature and up to $\sim$5 K the thermopower decreases almost linearly toward zero. The negative thermoelectric power indicates that the material is an *n*-type (electron) conductor. These properties suggest that Ba_6Ge_{24} is most likely a metal or a degenerate semiconductor.

The anomalous transition of the electrical conductivity and the Seebeck coefficient seem to be related to the Ge vacancies. For comparison, electrical conductivity and thermoelectric power of polycrystalline ingots of $Ba_6Ge_{21.93}In_{3.07}$ and $Ba_6Ge_{23.32}Sn_{1.68}$ were measured as a function of temperature and do not show anomalous behavior, see Fig. 5. Both compounds show metallic properties. The room temperature electrical conductivities of $Ba_6Ge_{21.93}In_{3.07}$ and $Ba_6Ge_{23.32}Sn_{1.68}$ were 1200 and 1700 S/cm, respectively, and the values increase with decreasing temperature. The values of thermoelectric power for $Ba_6Ge_{21.93}In_{3.07}$ and $Ba_6Ge_{23.32}Sn_{1.68}$ were -32 and -14 μV/K, respectively, at room temperature and decrease linearly with decreasing

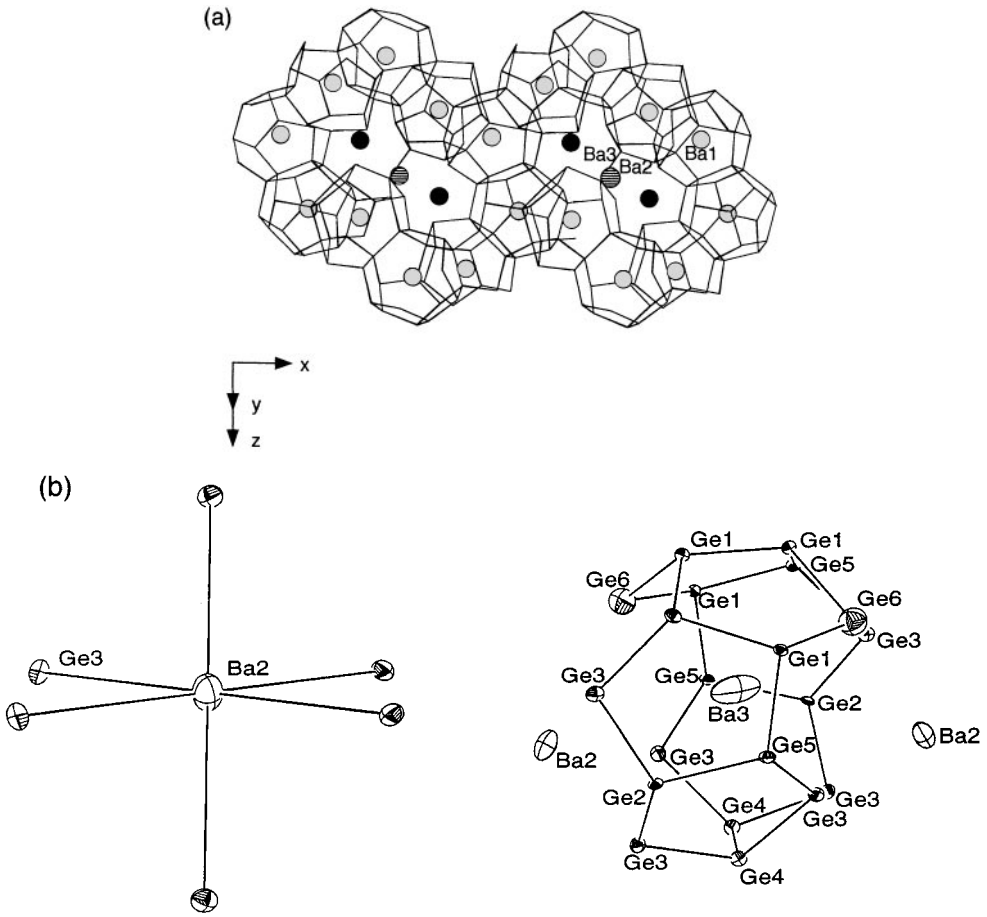

FIG. 3. (a) Local environment of Ba(2) and Ba(3) atoms. The channels filled by Ba(2) and Ba(3) atoms exist between helical chains. (b) ORTEP representation of the environment around Ba(2) and Ba(3). The six Ge atoms around these barium atoms are at a distance of 3.426 Å.

temperature. Since no evidence of vacancies was indicated in the structural refinement of $Ba_6Ge_{21.93}In_{3.07}$ and $Ba_6Ge_{23.32}Sn_{1.68}$, the existence of extra electrons in the conduction band is expected. Since In has one less electron than Ge, there is still one extra electron per formula unit to balance the charge. Therefore, the metallic characteristics on the electrical conductivities observed in both compounds are not surprising. To get a semiconductor, the stoichiometric compound of $Ba_6Ge_{21}In_4$ is needed (15).

The total thermal conductivity was measured on elongated ingot samples of Ba_6Ge_{24} and showed a significant contribution from radiative losses at higher temperatures (i.e., 140–300 K). The measured value at room temperature was $\sim 2.8\ W/m \cdot K$ (Fig. 6). The thermal conductivity exhibits a minimum at 120 K and then rises to a maximum peak at 15 K before it falls toward zero at ~ 0 K. The substantial rise in thermal conductivity between 140 and 300 K is attributed to radiation losses originating from the sample shape and from the electronic contribution to the thermal conductivity, which follows the Wiedemann–Franz law (16). The measured thermal conductivity can be written as

$$\kappa_{meas} = \kappa_{latt} + \kappa_{el} + \kappa_{rad},$$

where κ_{meas} is the measured value, κ_{latt} is the lattice contribution, κ_{el} is the electronic contribution, and κ_{rad} is the apparent enhancement due to radiation losses. The latter term increases linearly with T^4 and thus becomes important at high temperatures. From the electronic conductivity data the κ_{el} was calculated to be $1.44\ W/m \cdot K$ using the Wiedemann–Franz law. The κ_{latt}, which follows a $1/(A + BT)$ dependence, was modeled based on the assumption that radiation losses are negligible below 140 K (16). Thus the κ_{rad} was obtained from $\kappa_{meas} - (\kappa_{latt} + \kappa_{el})$ and it was estimated at $0.94\ W/m \cdot K$. Thus the total thermal conductivity of the bulk sample is $\sim 1.9\ W/m \cdot K$. Given that, the electronic contribution κ_{el} is $1.44\ W/m \cdot K$; this gives a lattice contribution of $0.50\ W/m \cdot K$, a very low value indeed. We note that it is only the κ_{latt} which is

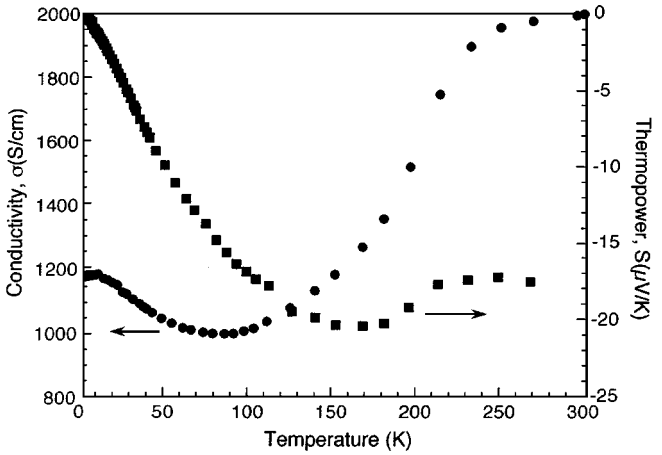

FIG. 4. Temperature dependence of the electrical conductivity and thermopower for a polycrystalline ingot of Ba_6Ge_{24}.

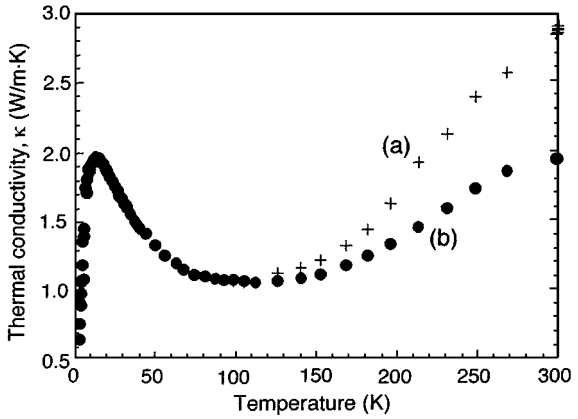

FIG. 6. Temperature dependence of the thermal conductivity of a polycrystalline ingot of Ba_6Ge_{24}. (a) Measured thermal conductivity; (b) thermal conductivity corrected for radiative losses.

sensitive to lattice and structural features of the compound. Therefore, from the very low value of κ_{latt} we can conclude that the presence of the rattling Ba^{2+} ions in the structure as well as the extensive presence of Ge vacancies do indeed contribute to reduce the lattice thermal conductivity of Ba_6Ge_{24}.

Of course, we note that values of electrical conductivity and thermopower are not intrinsic to the material, but rather reflect its electronic doping state. If there is a way to reduce the electrical conductivity, i.e., reduce the number of carriers, then we can expect a high thermopower and a significantly lower total thermal conductivity by virtue of the lower κ_{el}. This could be achieved by gaining good control of the material's stoichiometry by introducing doping agents or by synthesizing appropriate derivatives. The lattice thermal conductivity can be expected to be reduced even further by partially substituting Ba with smaller and heavier cations, such as Eu. Efforts to fully characterize the thermoelectric properties in these and similar Zintl phases are now underway.

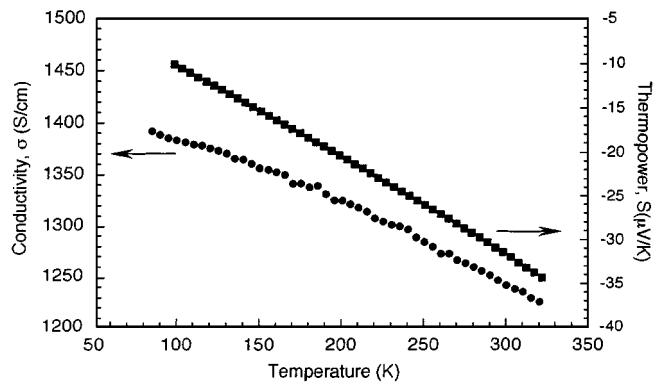

FIG. 5. Temperature dependence of the electrical conductivity and thermopower for a polycrystalline ingot of $Ba_6Ge_{21.93}In_{3.07}$.

ACKNOWLEDGMENTS

Financial support from DARPA through the Army Research Office (DAAG55-97-1-0184) and the Center for Fundamental Materials Research are greatefully acknowledged. S.-J.K. also acknowledges financial support from the Korean Ministry of Education (BSRI 96-3413).

Note Added in Proof. While this manuscript was under review the crystal structure of Ba_6Ge_{25} was reported. (a) W. Carrillo-Cabrera, J. Curda, H. G. von Schnering, S. Paschen, and Y. Grin, *Z. Kristallogr.-New Cryust. Str.* **215(2),** 207–208 (2000). (b) H. Fukuoka, K. Iwai, S. Yamanaka, H. Abe, K. Yoza, and L. Haming, *J. Solid State Chem.* **151,** 117 (2000).

REFERENCES

1. (a) G. A. Slack, *in* "CRC Handbook of Thermoelectrics" (D. M. Rowe, Ed.), p. 407.Chemical Rubber, Boca Raton, FL, 1995. (b) G. S. Nolas, G. A. Slack, D. T. Morelli, T. M. Tritt, and A. C. Ehrlich, *J. Appl. Phys.* **79,** 4002 (1996). (c) G. A. Slack, *Solid State Phys.* **34,** 1 (1979).
2. (a) G. S. Nolas, J. L. Cohn, G. A. Slack, and S. B. Schujman, *Appl. Phys. Lett.* **73,** 178 (1998). (b) G. S. Nolas, J. L. Cohn, and G. A. Slack, *Phys. Rev. B* **58,** 164 (1998). (c) G. S. Nolas, T. Weakley, and J. L. Cohn, *Chem. Mater.* **11,** 2470 (1999). (d) B. C. Sales, B. C. Chakoumakos, D. Mandrus, and J. W. Sharp, *J. Solid State Chem.* **146,** 528 (1999). (e) N. P. Blake, L. Mollnitz, G. Kresse, and H. Metiu, *J. Chem. Phys.* **111,** 3133 (1999).
3. (a) G. A. Slack, *in* "Thermoelectric Materials—New Directions and Approaches" (T. Tritt, M. G. Kanatzidis, H. Lyon, and G. Mahan, Eds.), *Mater. Res. Soc. Symp. Proc.* 478, p. 47. Mater. Res. Soc., San Francisco, CA, 1997.
4. (a) J. S. Kasper, P. Hagnemuller, M. Pouchard, and C. Cros, *Science* **150,** 1713 (1965). (b) C. Cros, M. Pouchard, P. J. Hagnemuller, and J. S. Kasper, *Bull. Soc. Chim. Fr.* 2737 (1968); *J. Solid State Chem.* **2,** 570 (1970). (c) C. Cros, M. Pouchard, and P. Hagnemuller, *J. Solid State Chem.* **2,** 570 (1970). (d) J. Gallmeier, H. Schäfer, and A. Weiss, *Z. Naturforsch. b* **24,** 665 (1969). (e) B. Eisenmann, H. Schäfer, and R. Zagler, *J. Less-Common Metals* **118,** 43 (1986). (f) B. Kuhl, A. Czybulka, and H.-U. Schuster, *Z. Anorg. Allg. Chem.* **621,** 1 (1995).

(g) A. Czybulka, B. Kuhl, and H.-U. Schuster, *Z. Anorg. Allog. Chem.* **594,** 23–28 (1991). (h) J. Dünner and A. Mewis, *Z. Anorg. Allg. Chem.* **621,** 191 (1995) (i) S. Bobev and S. C. Sevov, *J. Am. Chem. Soc.* **121,** 3795 (1999).
5. (a) J.-T. Zhao and J. D. Corbett, *Inorg. Chem.* **33,** 5721–5726 (1994) (b) T. F. Fässler and C. Kronseder, *Z. Anorg. Allg. Chem.* **624,** 561 (1998). (c) T. F. Fässler, *Z. Anorg. Allg. Chem.* **624,** 569 (1998). (d) R. Kroner, R. Nesper, and H. G. von Schnering, *Z. Kristallogr.* **182,** 164 (1988). (e) H. G. von Schnering, R. Kröner, W. Carillo-Cabrera, K. Peters, and R. Nesper, *Z. Kristallogr.* **213,** 665 (1998).
6. "Structure and Bonding of Zintl Phases and Ions" (S. M. Kauzlarich, Ed.). VCH, New York, 1996.
7. H. Schäfer and B. Eisenmann, *Rev. Inorg. Chem.* **3**(29), 101 (1981).
8. S. J. Kim, S. Hu, C. Uher, and M. G. Kanatzidis, *Chem. Mater.* **11,** 3154 (1999).
9. B. Chen, C. Uher, L. Iordanidis, and M. G. Kanatzidis, *Chem. Mater.* **9,** 1655 (1997).
10. SMART, Siemens Analytical X-Ray System, Inc., Madison, WI, 1994.
11. SAINT, Version 4, Siemens Analytical X-Ray System, Inc., Madison, WI, 1994.
12. Sheldrick, G. M. University of Göttingen, Germany, to be published.
13. Sheldrick, G. M. SHELXTL, Version 5, Siemens Analytical X-Ray Systems, Inc., Madison, WI, 1994.
14. F. D. Rosi, B. Abeles, and R. V. Jengen, *J. Phys. Chem. Solids* **10,** 191 (1959).
15. H. G. von Schnering, R. Kroner, W. Carrillo-Cabrera, K. Peters, and R. Nesper, *Z. Kristallogr.-New Cryst. Str.* **213(4),** 665 (1998).
16. H. M. Rosenberg, "The Solid State," 2nd Ed., p. 95. Clarendon Press, Oxford, 1978.